Structure of *Salmonella typhimurium nrdF* Ribonucleotide Reductase in Its Oxidized and Reduced Forms[†,‡]

Mathias Eriksson, Albert Jordan,[§] and Hans Eklund*

Department of Molecular Biology, Swedish University of Agricultural Sciences, Uppsala Biomedical Center, Box 590, S-751 24 Uppsala, Sweden, and Department of Genetics & Microbiology, Autonomous University of Barcelona, E-08193 Barcelona, Spain

Received June 11, 1998; Revised Manuscript Received July 22, 1998

ABSTRACT: The first class Ib ribonucleotide reductase R2 structure, from *Salmonella typhimurium*, has been determined at 2.0 Å resolution. The overall structure is similar to the *Escherichia coli* class Ia enzyme despite only 23% sequence identity. The most spectacular difference is the absence of the pleated sheet and adjacent parts present in the *E. coli* R2 structure; the heart-shaped structure loses its tip. From sequence comparisons, it appears that this feature is shared with all other class Ib enzymes and, in this respect, is more like the mammalian class Ia enzymes. Both the oxidized and reduced iron forms have been investigated. In the ferric iron center, both iron ions are octahedrally coordinated and bridged by one carboxylate and one oxide ion. The ferrous form has lost the bridging oxide ion but is bridged by two carboxylates. Accompanying the change in redox state, helix E changes its conformation from one covering the metal center in the oxidized form to a more open reduced form. A narrow channel is opened which may permit easier access of oxygen to the ferrous iron site and to efficiently generate the tyrosyl radical.

Ribonucleotide reductases (RNR) are uniquely responsible for de novo production of deoxy nucleotides for DNA synthesis (*1*). An intricate allosteric regulation enables the enzyme to reduce all four types of ribonucleotides and produce a balanced pool of deoxyribonucleotides. Different organisms have tuned their RNRs to adjust their production of DNA precursors to the particular base composition of their genome (*2*). Imbalances are associated with different genetic effects as well as an increased sensitivity to DNA damaging agents (*3*−*9*). Two redox equivalents, in most cases delivered from NADPH, are consumed for every substrate reduction. Furthermore, the catalysis requires an organic free radical to activate the substrate before reduction.

The composition of subunits varies between species, but all RNRs appear to share a similar large subunit containing the active site, allosteric regulatory binding sites, and redox active cysteines (*10, 11*). The radical can be produced in at least three completely different ways and has led to the division of RNR into different classes (*10*). The class I enzymes contain a protein with a diiron center which is used to generate a tyrosyl radical with the help of oxygen (*12*). The class II reductases contain no radical-generating protein. Instead, the radical is formed by cleaving the Co−adenosyl bond in adenosylcobalamin (*13*). For the anaerobic class III enzymes, a glycyl radical is generated by the homolytic cleavage of *S*-adenosylmethionine with an electron coming from an iron−sulfur cluster in its dimeric small subunit (*14, 15*).

The most well-studied are the class I enzymes which are present in all eukaryotes and in some bacteria (like *Escherichia coli* and *Salmonella typhimurium*). These enzymes are organized as two soluble homodimers: R1 (2 × 761 residues in *E. coli*) and R2 (2 × 375 residues in *E. coli*). R1 contains the active site and redox active cysteines as well as the allosteric binding sites (*1, 10*). One of the allosteric sites, the specificity site, regulates the specificity at the active site by binding different deoxyribonucleotide triphosphates or adenosine triphosphate. The result of this regulation tunes the enzyme to produce a balanced pool of deoxyribonucleotides. The second allosteric site, the activity site, regulates the activity of the enzyme. ATP activates the enzyme while dATP inhibits it. The active site contains redox active cysteines responsible for substrate reduction (*16*−*18*). These cysteines are reduced for each enzymatic cycle by thioredoxin or glutaredoxin with the help of C-terminal R1 cysteines as a shuttle for reducing equivalents (*19*).

R2 is responsible for generating and storing the organic free radical and contains the iron center in close proximity to the stable tyrosyl radical. The structure of *E. coli* R2 revealed that the enzyme contains a diferric center in each subunit. The two irons are bridged by a μ-oxo bridge. In addition they are liganded by four carboxylate side chains, two histidines, and two waters. The buried tyrosine 122 storing the radical is surrounded by hydrophobic residues and is close to one of the carboxylate iron ligands. The iron site and tyrosine radical are embedded between the four long helices (denoted B, C, E, and F) of a helical bundle. The

[†] This work was supported by grants from the Swedish Natural Science Research Council and the Swedish Cancer Foundation (to H.E.).

[‡] The atomic coordinates described in this paper have been deposited in the Brookhaven Data Bank (entries 1r2f and 2r2f).

* To whom correspondence should be addressed. Tel: 46-18 471 45 59. Fax: 46-18 53 69 71. E-mail: hasse@xray.bmc.uu.se.

[§] Autonomous University of Barcelona.

S0006-2960(98)01380-4 CCC: $15.00
Published on Web 09/05/1998

tyrosyl radical can be scavenged by hydroxyurea and other radical scavengers to give metR2 with a ferric iron center and a normal tyrosine. The active form of R2 can be regenerated from metR2 by reduction of the irons to the diferrous state. In vivo, a flavin reductase system appears to play an important role in the reduction of the irons (*20*). The tyrosyl radical is generated by the activation of molecular oxygen. Of the four electrons needed for activation, two come from the ferrous atoms and one comes from Tyr122. The last electron required to reduce the oxygen molecule is derived from an external source.

Recently, a second RNR was found in *S. typhimurium* and later also in *E. coli*. (*21*−*23*). The genes for these enzymes were labeled *nrdE* and *nrdF*. These enzymes have the same subunit composition and show significant sequence homology to the normal class I enzymes but lack allosteric overall activity regulation (*24*). They contain an antiferromagnetically coupled diiron site with a tyrosyl free radical but differ in the EPR spectrum of the tyrosyl radical, suggested to be caused by changes in side-chain torsion angles (*25*). Furthermore, this group of reductases utilizes a different small redox protein similar to thioredoxin and glutaredoxin. It is usually present in the same operon as the *nrdE* and *nrdF* genes together with a fourth protein of unknown function (*23*, *26*). Class I was thus subdivided into Ia and Ib and the class Ib subunits are called R1E and R2F (originating from the gene names *nrdE* and *nrdF*). The class Ib enzyme is fully functional in *E. coli* and *S. typhimurium* but does not appear to be essential in these organisms (*27*). The reason for having two functional class I enzymes is not understood. Whereas the class Ia enzymes are present in both eukaryotes and some bacteria, class Ib reductases are more commonly distributed among prokaryotes. The class Ib enzyme is present as the active aerobic enzyme in *Mycobacterium tuberculosis* (*28*), *Lactococcus lactis* (*29*), and *Bacillus subtilis* (*30*); the gene has also been found in *Mycoplasma genitalium* (*31*) and *Mycoplasma pneumonia* (*32*). Biochemical and genetic data of the manganese-containing ribonucleotide reductase from *Corynebacterium ammoniagenes* (*33*) indicate that it belongs to the class Ib enzymes (*34*).

Because of occurring in pathogenic bacteria, class Ib enzymes have attracted an increased attention. We report here the first structure of a class Ib R2F protein. Structures of both the oxidized and reduced iron site have been determined. The redox change causes a change in the diiron metal coordination and also a conformational change in one of the internal helices.

MATERIAL AND METHODS

Overexpression of the S. typhimurium R2F Protein. For obtaining large amounts of R2F protein a T7 RNA polymerase-dependent expression system was used. Expression vector pET24a (Novagen) was used, taking advantage of the fact that the *nrdF* gene from *S. typhimurium* is flanked by two *Nde*I restriction sites (5′-CATATG-3′), the first containing the translation start ATG codon. This plasmid contains an *Nde*I site downstream of a strong ribosome binding site preceded by a T7 promoter. Cloning of genes by its translation start codon into the *Nde*I site allows high-level expression when the T7 RNA polymerase is induced by the addition of IPTG in the host strain BL21(DE3) (Novagen). A DNA fragment of 1.7 kb containing the *nrdF* coding region was obtained by *Nde*I digestion of plasmid pUA335 containing the *S. typhimurium nrdHIEF* operon (*21*), gel-purified, cloned into the plasmid pET24a digested with the same restriction enzyme, and dephosphorylated with alkaline phosphatase. The ligation mix was transformed into *E. coli* DH5αF′ (Clontech Lab. Inc.), and several resulting clones were checked to contain the desired insert and to be in the right transcription orientation with respect to the T7 promoter through restriction analysis with enzymes *Nde*I and *Hin*dIII, respectively. Plasmid (pUA727) from one clone, unambiguously confirmed to code for *nrdF*, was transformed to *E. coli* BL21(DE3) cells. General cloning procedures were carried out by standard methods (*35*). Restriction enzymes and other enzymes were from Boehringer Mannheim.

Purification. E. coli BL21(DE3) cells containing pUA727 were grown at 37 °C in Luria broth containing kanamycin at 50 μg/mL to mid-log phase (OD_{550} of 0.6). The cells were induced by 1 mM IPTG, and growth was continued for 3 h before harvest. The procedure to purify the *nrdF* protein is similar to that described (*22*). A typical cell growth of 4 L of culture gave approximately 16 g of wet cells. A mixture of 50 mM TRIS, pH 7.6, 20 mM DTT, 1 mM PMSF and lysozyme were added to the cells, and the resuspended mix was sonicated to lyse the cells. DNA was removed by adding streptomycin sulfate to a final concentration of 1%. The protein in the supernatant was precipitated by 70% saturated ammonium sulfate. The ammonium sulfate pellet was resuspended in 50 mM TRIS, pH 7.5, 20 mM DTT and dialyzed overnight. The dialysate was applied to a DEAE-FF (Pharmacia Biotech) column. The elution of R2F could be followed spectroscopically at 370 or 410 nm proving the existence of the iron site and a tyrosyl radical. The total amount of *nrdF* protein is close to one-half of the total cellular amount (Figure 1). The protein was >95% pure and was concentrated to 100−200 mg/mL using a Centricon 30 concentrator.

Crystallization and Data Collection. The protein solution was made in 50 mM TRIS, pH 7.5, 10 mM DTT with protein concentrations varying between 10 and 30 mg/mL. Crystals grew in hanging drops over a reservoir containing 15−25% PEG8000, TRIS, pH 8−8.5, and 0.7 M NaAc at 15 °C. The crystals grow to a size of 2 × 1 × 0.3 mm after 3−6 days. The crystals were cryoprotected in 15% PEG400 + the reservoir solution and then removed by a fiber loop and immediately flash-cooled in liquid nitrogen. Intensity data were collected from crystals using a cryosystem (Oxford Cryosystem or MRC) using image plate scanners (MAR-Research Hamburg or Raxis IIc) and graphite monochromatized Cu Kα radiation from a RU 200 rotating-anode generator (Rigaku, Tokyo, Japan) or synchrotron radiation at EMBL Hamburg (station BW7b) or ESRF Grenoble (BM14). Diffraction images were processed and scaled using the HKL program package (*36*). Details of the data collection are summarized in Table 1.

The crystals are primitive monoclinic and could, by the systematic absences, be assigned to the space group $P2_1$. The cell parameters are $a = 58$ Å, $b = 72$ Å, $c = 96$ Å, and $\beta = 95°$. The asymmetric unit contains one dimer with a calculated solvent content of 50%.

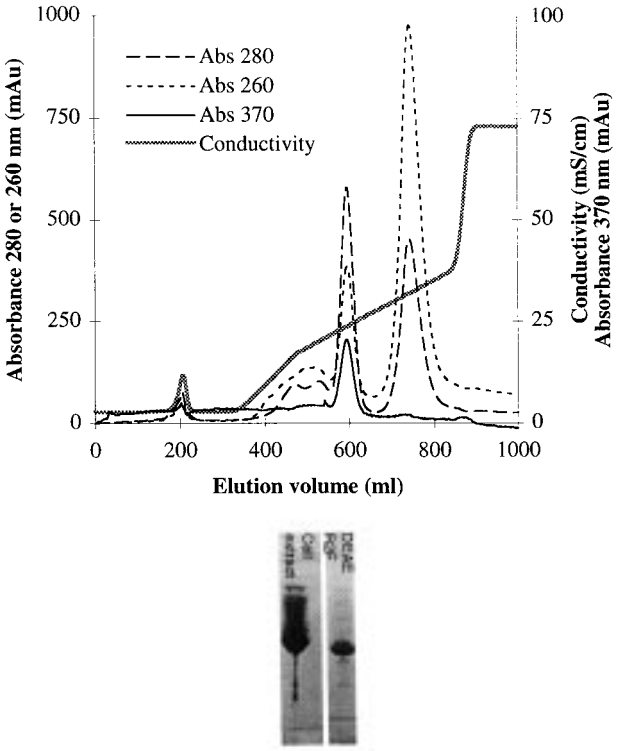

FIGURE 1: Chromatogram and SDS−PAGE from the purification of R2F. An ammonium sulfate dialyzed cell lysate appplied to a DEAE FF (Pharmacia Biotech) column and eluted with 0−1 M KCl.

Table 1: Data and Refinement Statistics[a]

	oxidized	X-ray reduced	chemically reduced	NO soak
data collection	BW7b	BW7b	BM14	BW7b
resolution of data	20−2.25	20−2.0	40−2.3	30−2.1
completeness, %	99.4 (99.5)	98.6 (98.2)	88.3 (89.9)	96.6 (93.8)
R_{sym}	6.6 (25.3)	7.2 (25.2)	4.8 (24.6)	6.9 (23.0)
completeness, $>2\sigma$	88.5 (70.7)	85.5 (60.2)	73.4 (44.9)	83.1 (59.4)
redundancy	3.3 (3.0)	3.1 (2.4)	2.0 (1.9)	3.4 (2.8)
refinement				
R_{work}	22.8	24.9	23.2	22.6
R_{free}	26.8	26.8	27.6	24.7
water molecules	415	355	397	397
protein atoms	4583	4594	3957	3957
B average	47.9	44.4	47.0	42.8
protein subunit A/B	36.9/58.9	34.0/55.4	35.4/58.6	31.5/53.7
Fe subunit A/B	35.0/47.1	33.0/47.1	45.6/67.7	31.6/42.2
solvent	48.5	41.3	46.8	44.6
rmsd				
bonds (Å)	0.07	0.07	0.07	0.07
angles (deg)	1.2	1.2	1.2	1.2

[a] BW7b, EMBL outstation in Hamburg, station BW7b; BM14, ESRF Grenoble, station BM14. Figures in parentheses are for the outer shell.

Heavy Atom Derivatives and Phasing. Molecular replacement trials were initially unsuccessful. Instead screens for heavy atom derivatives were made. The heavy atom compounds were dissolved in the reservoir solution. The crystals were soaked 18−36 h in 1−5 mM heavy atom concentration. The EMTS derivative contained two principal sites that could readily be located in the difference Patterson map (15−4.0 Å) by using RSPS (*37*). Other heavy atom positions from minor positions in the EMTS data, $PtCl_4^{2-}$ and $Au(CN)_2^-$ derivatives, were located in difference Fourier maps and verified in the difference Patterson maps. Heavy atom parameters were refined using the program SHARP (*38*). Final statistics are presented in Table 2. The resulting MIR phases were improved by solvent flattening using SOLOMON (*39*); the map revealed the two subunits allowing for a further map improvement by density modification including averaging using DM (*40*).

Model Building and Refinement. The atomic model was constructed using the program O (*41*) and refined against the 2.25 Å data using maximum likelihood implementation in the β-test version of the program CNS (Axel Brünger, personal communication) (*42*−*47*). The initial model had an *R* factor of 0.38 for data from 20.0 to 2.7 Å. After one round of simulated annealing, followed by three iterations of conventional refinement and model building, the *R* factor still remained high ($R = 0.32$, $R_{free} = 0.35$). Anisotropic scaling brought down the *R* factors significantly (0.24 and 0.27, respectively), and the data could be extended to 2.25 Å. After five more iterations of refinement and model building, the final R_{work} and R_{free} were 0.23 and 0.27, respectively. The occupancy of the irons was refined by fixing the temperature factors to the average of the iron coordinating atoms in each site. The final modeling of the diiron centers was done in simulated annealing omit maps. A summary of the final refinement statistics is presented in Table 1.

Reduced R2F. Reduced R2F was obtained by three different methods: (1) Reducing the protein in the crystalline state by addition of a 3% sodium dithionite solution containing 1 mM phenosafranin in an anaerobic box ($O_2 <$ 2 ppm). After 3 h, the crystals were frozen as described above with the addition of 3% sodium dithionite and 1 mM phenosafranin in the cryogenic solution. (2) The protein was reduced chemically by 3% sodium dithionite and 1 mM phenosafranin, crystallized anaerobically, and frozen as the previously reduced crystal. (3) Aerobically grown crystals were soaked in a cryoprotectant solution containing 20% glycerol before the flash freeze. The protein was reduced in an intense X-ray beam at BW7b in EMBL outstation Hamburg DESY.

RESULTS AND DISCUSSION

Expression and Purification of R2F. The *nrdF* gene from *S. typhimurium* coding for a class Ib R2 protein (R2F) was introduced into a T7 RNA polymerase-dependent expression system in *E. coli*. The system produced large amounts of R2F protein. A single chromatographic purification step produces a protein more than 95% pure. The elution of R2F was monitored at 370 and 410 nm showing that the protein contains both an iron metal center and a tyrosyl radical characteristic of an R2 ribonucleotide reductase protein (Figure 1).

Structure of R2F. Monoclinic crystals of *S. typhimurium* diferric R2F were used for the structure determination using multiple isomorphous replacement (MIR). All data were collected at 100 K. The structure was determined at 2.1 Å and refined to a crystallographic *R* factor of 0.226 and R_{free} of 0.247. All residues are in allowed regions of the Ramachandran plot (Figure 2), and the geometry of the final model is good (Table 2). The crystals contain two subunits in the asymmetric unit and were refined using restraints in the earlier stages. The electron density is very well-defined in the A subunit except for the first 3−5 residues and the

Table 2: Data Collection and Phasing Statistics

compd	soak (mM/h)	resolutn (Å)	compl. (%)	R_{merge} (%)	R_{iso} (%)	sites	FH/ϵ acentric/centric	RCullis acentric/centric
Native		2.3	99.4					
Hg	1.6/30	3.2	88.1	11.0	30.2	8	1.96/1.77	0.72/0.75
Pt	2.0/24	3.0	95.1	9.5	18.1	6	0.66/0.63	0.93/0.92
Au	0.6 /36	3.4	97.6	11.7	15.8	8	1.78/1.46	0.77/0.83

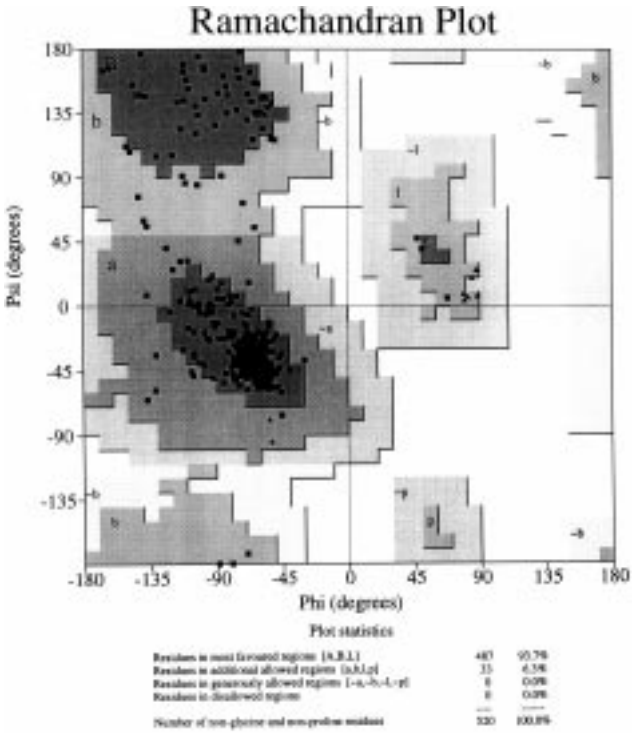

FIGURE 2: Ramachandran plot for the residues in the R2F dimer.

last 30−33 C-terminal residues. The flexibility of the C-terminus is a common property of the R2 proteins (*48*−*52*). This part is essential for R1−R2 holoenzyme formation. In the B subunit there are a few additional regions with poor density, particularly the end of helix αE, the end of helix αG, the beginning of αH, and the loop connecting these two latter helices and the C-terminal residues. These poor density regions are located at one edge of the molecule. This may be related to packing variations that affect these residues at the tip of one side of the molecule. The temperature factors are as a consequence high in the $x-y$ plane when z is about 0.

R2F is a helical protein and contains no β-sheet. The general fold is similar to other R2 proteins (*48, 49, 52*), and all helices in the main helical bundle, αA−αH, are present in R2F (Figure 3). However, one of the four small helices perpendicular to the main bundle, α3, is missing, and instead helix αG starts immediately after αF and is slightly longer than in *E. coli* R2. The organization of the subunits in the dimer is also very similar to other R2 proteins. The absence of the pleated sheet strands of *E. coli* R2, a gap of 32 residues, makes the general appearance more similar to mouse R2 (*52*). The appealing heart shape of the *E. coli* R2 is obviously the unusual form for R2 proteins.

Comparison with Other R2 Structures. Two hundred forty-two Cα atoms in the structure of an R2F subunit superimpose on the mouse R2 structure with an rms fit of

FIGURE 3: Dimeric R2F structure is viewed such that the left subunit is shown roughly along the directions of the helices and the right subunit is shown roughly perpendicular to the helix bundle. The iron atoms in the dinuclear centers are shown as black spheres. The nomenclature is adopted after that in ref *48*. This figure and most of the others were generated with BOBSCRIPT, Robert Esnouf's extended version of MOLSCRIPT (*62*).

1.7 Å using standard parameters in O (*41*). Similarly, 253 Cα atoms of each subunit of R2F can be superimposed on *E. coli* R2 subunits with an rms fit of 1.8 Å. These figures are roughly equivalent, and in view of the general shape, the R2F dimer appears more similar to mouse R2 than *E. coli* R2 (Figure 4). This is surprising since the sequences in the structural alignment show only 15.9% identities between R2F and mouse R2, compared to 22.8% identities between R2F and *E. coli* R2 (identities in the flexible C-terminus are included). The cores of the molecules are most similar. The side of the dimer that has been suggested to bind R1 is significantly more similar than the opposite side.

Different Oxidation States of the Iron Center. Four different high-resolution data sets have been collected, two with oxidized crystals and two with reduced crystals. One of the reduced crystals was crystallized in an anaerobic box with NO added; the second was reduced chemically by the addition of dithionite. The reduced environment was monitored by the absence of oxidized (violet) phenosafranine.

Structure of the Iron Site in Ferric R2F. The iron atoms of the ferric R2F are ligated by two histidines, three glutamates, and one aspartate (Figure 5a). The two ferric ions are bridged by one of the glutamate residues and an O^{2-} ion. The distance between the two iron ions is 3.3 Å, and the distances between the O^{2-} ion and the iron ions are 1.8 Å. One water molecule appears in difference Fourier maps between the two irons, 2.5−2.6 Å from the iron atoms, and may be regarded as a ligand to both irons. The exact position of a water molecule may even at this resolution be

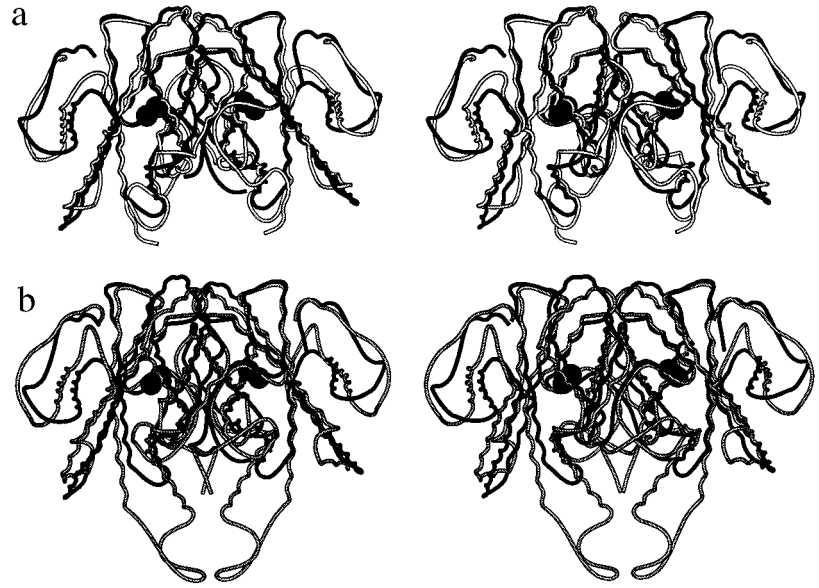

FIGURE 4: Superimposed main chain structures of R2s: (a) R2F (in black) and mouse R2 (in white); (b) R2F (in black) and *E. coli* R2 (in white). The iron atoms in the dinuclear centers of R2F are shown as black spheres.

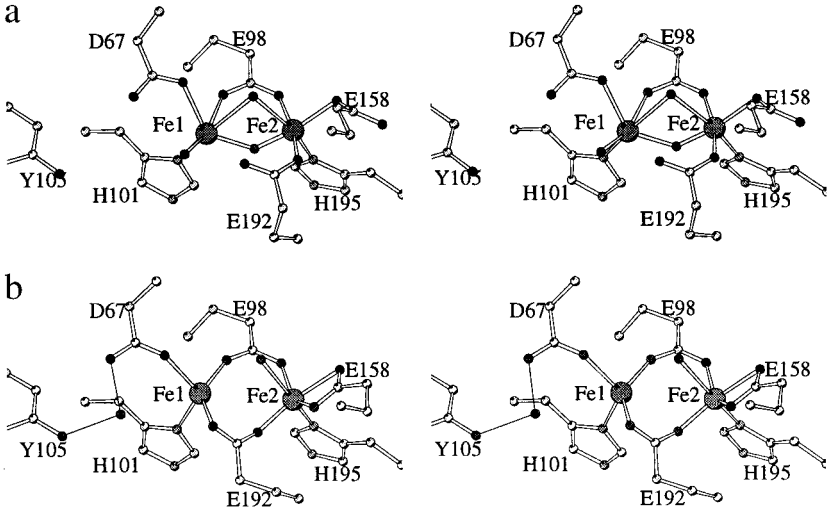

FIGURE 5: Dinuclear iron site coordination in its (a) oxidized and (b) reduced states.

disturbed by the close proximity of the electron-rich diiron atoms. With this water molecule bound to both iron atoms, the geometry of the coordination of both iron ions is roughly octahedral. The coordination of Fe2 is identical to that in the *E. coli* R2 structure. The Fe1 coordination differs: it has a monodentate carboxylate binding of Asp67, a shared water molecule with Fe2, and one additional water molecule. Similarities and differences also exist in the second ligand sphere. The sequentially first histidine ligand (His118 in *E. coli* numbering) is in all R2 structures hydrogen-bonded to an Asp that is further hydrogen-bonded to a conserved Trp. The sequentially second histidine (His241 in *E. coli* numbering) is hydrogen-bonded to a water molecule in a pocket in the structure. This pocket contains two additional water molecules hydrogen-bonded to Asn and Asp side chains and a main chain carbonyl. This arrangement is similar to that in the mouse R2, whereas the histidine in *E. coli* R2 is hydrogen-bonded to Ser and Gln side chains. This difference between the two latter structures has been suggested to be one of the reasons for the lower stability of the iron center of mouse R2 (*52*). This argument seems not relevant in view that the R2F structure has a stable iron center like *E. coli* R2. The iron sites in the refined R2F structure seem to be fully occupied as judged by temperature factors of iron atoms and ligands.

Reduced R2F. Both data sets of the reduced crystals are very similar, and the attempt to bind NO to one of these crystals was not successful; the resulting map (Figure 6) shows no extra features when compared to the map from the other reduced crystal. The bridging O^{2-} ion is not present in the reduced crystals (Figure 5b). Instead the two ferrous ions are bridged by two glutamate residues, and Glu109 has turned and become a bridging ligand. In contrast to the reduced *E. coli* R2 iron site, a water molecule is present bound to Fe2 and located 2.9 Å from Fe1. This situation is very similar to that of the manganese-substituted *E. coli* enzyme (*53*) but different from that of the reduced *E. coli* R2 which does not contain any iron-liganded water molecule (*54*). Without this water molecule, Fe1 is bound in a tetrahedral coordination, while Fe2 has a square-pyramidal coordination with Glu158 as a bidentate ligand in the same plane as Glu98 and Glu192 and with His195 at the tip of the pyramid. If this water molecule is considered a ligand, the Fe2 coordination is close to octahedral, while the Fe1

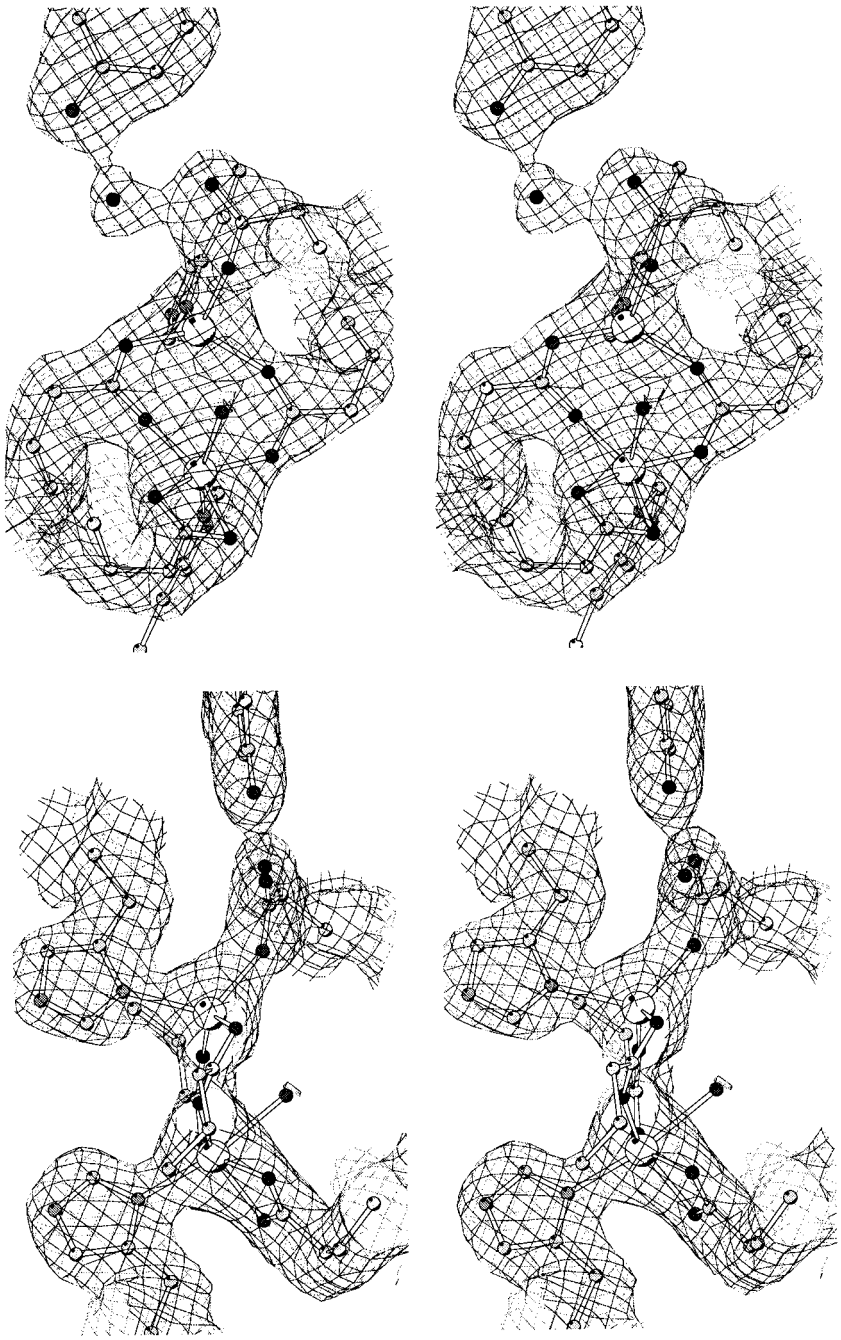

FIGURE 6: Electron density of the iron site in reduced R2F in two orthogonal views. The simmualted annealing $2F_o - F_c$ omit map is contoured at 1σ.

coordination is a distorted trigonal bipyramid. The distance between the two iron atoms in reduced R2F is 3.7 Å, which is shorter than that for *E. coli* R2 where the distance is 3.9 Å. Also in this respect, the reduced R2F is more like the Mn-substituted *E. coli* R2, where the intermetal distance is 3.6 Å.

The water molecule in the reduced R2F is facing the free side of the iron pair. The presence of a water at this position appears to be less favorable than the situation in the reduced *E. coli* R2. The water should be displaced from its position to allow the dioxygen to bind to the ferrous ions and transform the protein to an active, ferric, radical form.

Reduction of Crystals by Synchrotron Radiation. A high-resolution data set of the oxidized R2F was collected on the synchrotron in Hamburg to 2.0 Å resolution. However, when analyzed it turned out to have the characteristic iron coordination of the reduced enzyme. A difference between the conditions used for this crystal and other ferric R2F crystals was that glycerol was used as a cryoprotectant. Comparison of the first frames of the collected data with the later ones confirmed that the reduction of the crystals took place during exposure. The more accessible subunit B was more easily reduced than subunit A that has tighter crystal packing. There are no detectable differences in the crystal packing between the reduced and oxidized forms of the protein. This suggests that the protein can shift between the two redox states with only intramolecular changes. This might explain why these changes evidently occur even in cryocooled crystals.

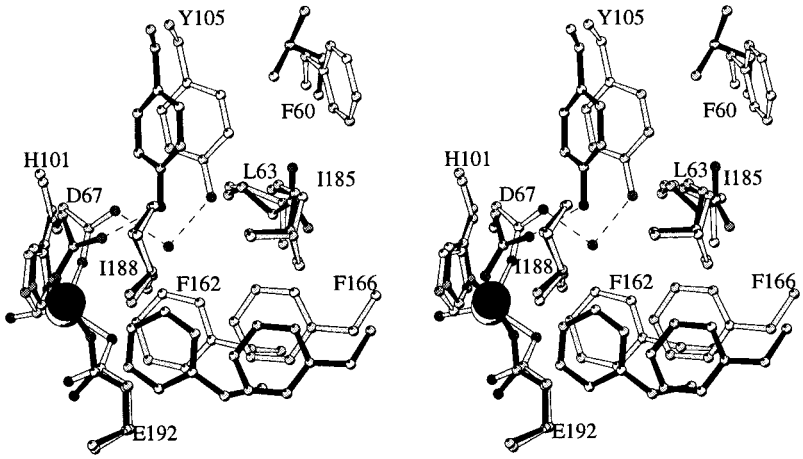

FIGURE 7: Superposition of the surroundings of the radical harboring tyrosine in the reduced forms of *E. coli* R2A (black) and *S. typhimurium* R2F (white). Cα atoms of the iron ligands were superimposed.

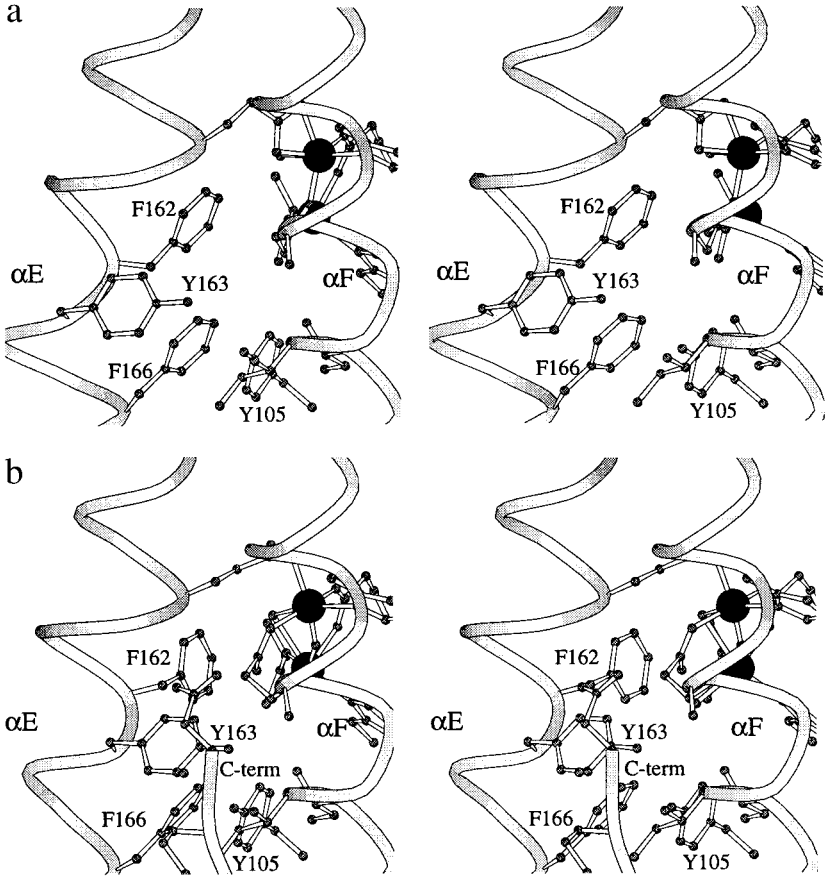

FIGURE 8: αE and αF helices in the (a) reduced and (b) oxidized forms of R2F. The conformation of αE in the reduced form is such that the active site becomes more accessible than in the oxidized form.

Reduction of the iron center by radiation has earlier been described for *E. coli* R2. γ-Irradiation of solutions containing up to 50% glycerol generated a mixed-valent $Fe^{3+}-Fe^{2+}$ state at 77 K (*55*). The rate of formation and the maximal amount of the mixed-valent state were highly dependent on the concentration of glycerol, an effective electron hole-trapping agent. A similar mixed-oxidation state was generated upon X-irradiation of a frozen aqueous solution of R2 at 77 K (*56*), although the yield was only 0.5% of the total protein rather than about 40% for γ-irradiation. This has been attributed to the absence of glycerol. It appears that a similar phenomenon was observed in crystals of *E. coli* R2 (54) and now in the R2F crystal frozen at 100 K in mother liquor containing glycerol, although in these cases a full two-electron reduction has taken place. The crystal used for determination of the reduced *E. coli* R2 structure at 100 K was not chemically reduced but a metR2 crystal allowed to return to room temperature after a short exposure to intense synchrotron X-irradiation at 100 K and subsequently refrozen (*54*). Reduction by X-ray diffraction has been reported also for the diiron center of Δ^9-stearoyl-acyl carrier protein desaturase (*57*).

Tyrosyl Radical Site. There is a significant difference in the position of the radical harboring tyrosine residue between R2F and *E. coli* R2. In all oxidized and reduced R2F subunits, the tyrosine side-chain hydroxyl is 6.5−7.0 Å away

from the closest iron. The corresponding distances are 5.2−5.3 and 4.8−4.9 Å for oxidized and reduced *E. coli* R2 subunits, respectively (Figure 7). The difference in side-chain conformation is due to a difference in χ_1 torsion angle plus a slight difference in helix conformation. The environment of the tyrosine side chain differs mainly in that a Leu and Phe in R2F substitutes a Gln and Leu, respectively, in *E. coli* R2 which are in van der Waals interactions with the tyrosine ring. In subunit A there is a clear density for a water molecule between the tyrosyl oxygen and the side chain of Asp67 which is not present in oxidized R2F. The situation is probably the same in subunit B, but the density is less good, and there is no distinct density for a water molecule. In the oxidized *E. coli* R2, there is no water molecule in this place, whereas in reduced *E. coli* R2, Asp84 forms a hydrogen bond to the side chain of Tyr122 (Figure 7).

Calculated proton hyperfine coupling constants for the β-protons show that the α-carbon is rotated 75−80° out of the plane of the ring in photosystem II and *S. typhimurium* RNR but only 20−30° in, e.g., *E. coli*, mouse, herpes simplex, and bacteriophage T4-induced RNRs (*58*). This qualitative difference agrees with the crystallographic structures, albeit the values differ slightly. The X-ray structures of oxidized and reduced R2F show values of 60−70° compared to 35−45° in the X-ray structures of oxidized and reduced *E. coli* R2.

The α*E Helix.* The αE helix is distorted in all R2 structures due to an extra residue in the helix, forming a π-type turn which distorts the hydrogen bonding of the helix. However, the distortions differ among earlier determined R2 structures (*52, 54*). In the electron density maps of the anaerobically grown R2F crystal, αE is well-defined. Difference Fourier maps between this structure and the oxidized structure show distinct features around the metal center, αE, and the C-terminus. The αE region is primarily one turn of helix between the two conserved phenylalanines (162 and 166 in R2F corresponding to 208 and 212 in *E. coli*) at a hydrophobic pocket between the radical harboring Tyr105 and the diiron site. The density of the oxidized R2F is disordered, but this section of the helix appears to undergo a conformational change where Tyr163 moves toward the C-terminus. Residues 164 and 165 move backward to allow for the tyrosine to move, and Phe162 changes rotamer (Figure 8). The rest of the E helix appears to be unaffected. The electron density for the C-terminus ends at residue 286 in the reduced structure, but in the oxidized structure it continues to Asn289. Tyr163 in its conformation in the oxidized structure is hydrogen-bonded to residue 288 stabilizing a few extra residues at the C-terminus.

The conformational changes of the E helix are very similar as those observed for the reduced *E. coli* R2 mutant where Ser211, which is a highly conserved residue in class Ia enzymes, was mutated to Ala (*54*). The residue corresponding to Ser211 in *E. coli* R2 is not conserved in the *nrdF* family of proteins but is a glycine instead. In the Ser211Ala mutant in *E. coli*, there is a movement of the side chain of Tyr209 (corresponding to Tyr163 in R2F) which in the mutant opens a channel into the R2 protein making the hydrophobic pocket and the diiron site accessible. Such a gating of the accessibility to the iron site would be very attractive if it could be related to the oxidation state of the iron center: open in the reduced form giving fast access of dioxygen to the iron site and closed in the oxidized form closing the access to the tyrosyl radical. However, no strict correlation to redox state has so far been possible to make. The R2F structure shows that the conformation in the reduced form is very similar to the open conformation in the Ser211Ala *E. coli* mutant structure. The oxidized structure appears to be more similar to the wild-type *E. coli* R2 protein. The entrance of the channel is further blocked in the oxidized state by the C-terminus interacting with Tyr163. Tyr163 is not conserved in eukaryotes where it mostly is a serine. The mouse R2 structure shows that this substitution forms a channel leading into the oxygen cavity of the R2 subunit probably explaining the higher susceptibility to radical scavengers of the mammalian enzyme (*52*).

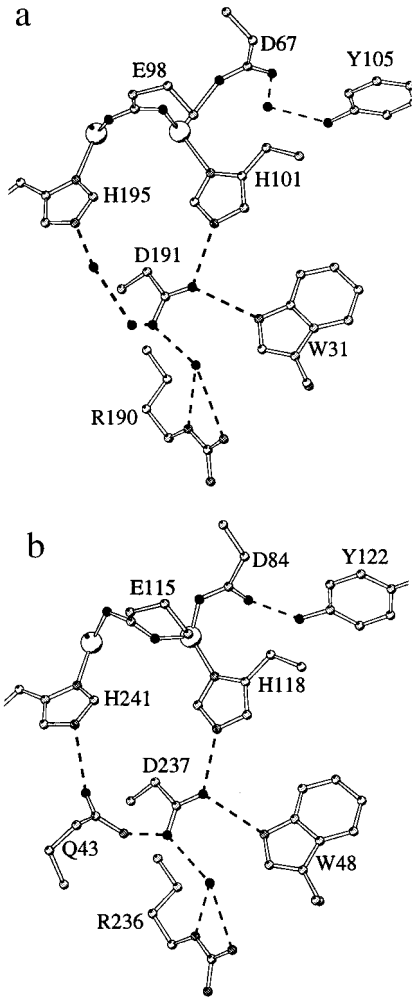

FIGURE 9: Hydrogen-bonded connections from the buried tyrosine to the surface which can be part of a radical transfer chain in (a) *S. typhimurium* R2F and (b) *E. coli* R2.

Radical Transfer Chain. A set of R2 residues has been implicated in the transfer of the radical from its stored position inside the R2 subunit to the active site in the R1 subunit (*48, 49*). These residues form an equivalent hydrogen-bonded chain in R2F that superimposes very closely in the two structures. The metal ligand His101 is hydrogen-bonded to Asp191 which is hydrogen-bonded to Trp31 with the same oxygen atom. The second oxygen of Asp 191 is hydrogen-bonded to a water molecule that is further hydrogen-bonded to a main chain carbonyl and the side chain Arg190 as in *E. coli* R2. This arginine (Arg236 in *E. coli* numbering) is the

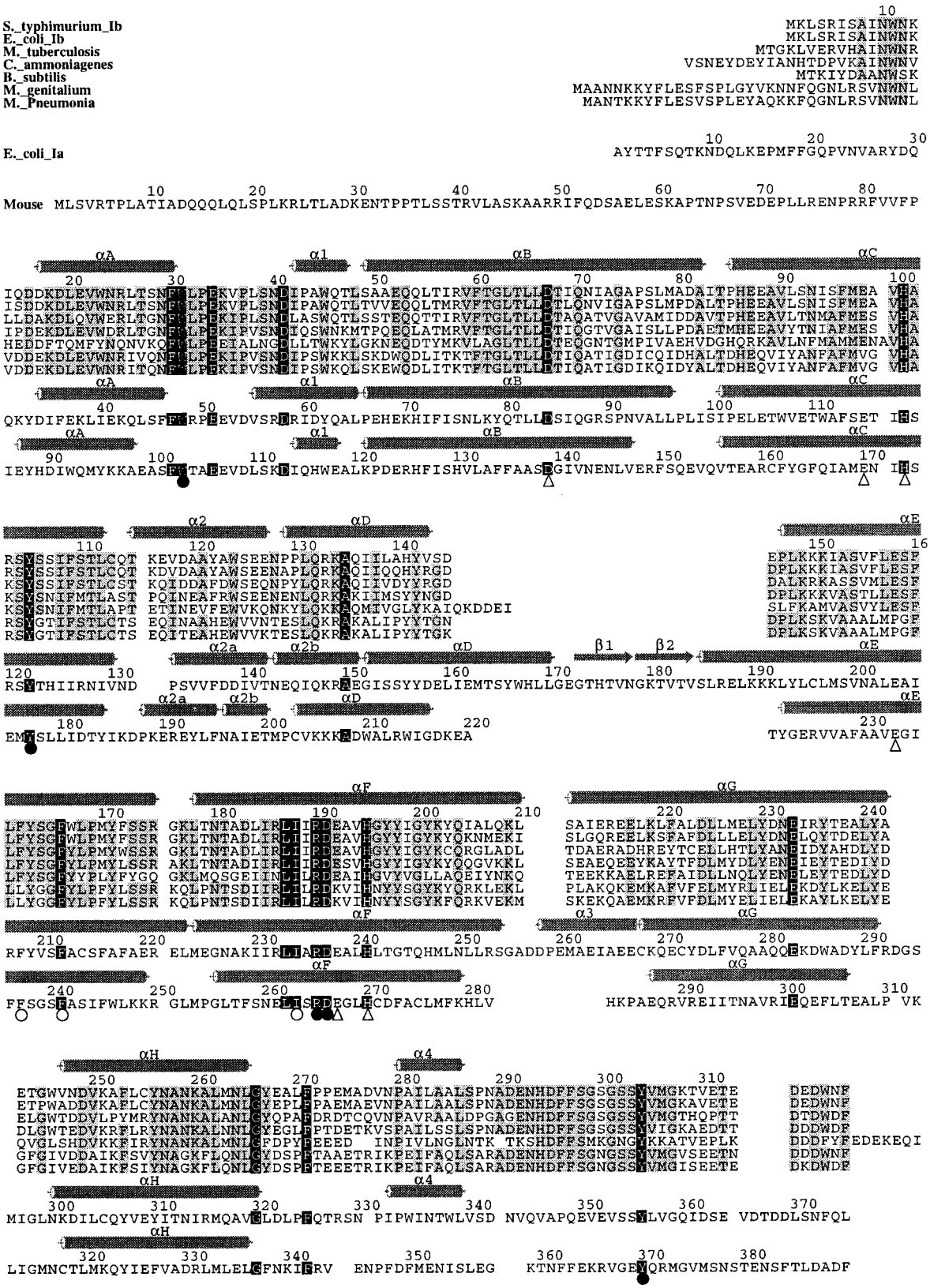

FIGURE 10: Structural alignment of *S. typhimurium* R2F sequence proteins to the Ia R2 proteins from *E. coli* and mouse and sequence alignment of the six other class Ib sequences. The secondary structure and sequence numbers are above the sequences. Residues conserved between the class Ib sequences and the two class Ia proteins are in black background, and conserved residues among class Ib enzymes are in gray background. Open triangles represent iron binding residues. Filled circles represent residues suggested to be involved in radical transfer. Open circles are residues at the hydrophobic pocket embedding the tyrosyl radical. Sequences were taken from Swissprot database (filenames in parentheses) *S. typhimurium* Ib (RIR4_SALTY), *B. subtilis* (RIR2_BACSU), *E. coli* Ib (RIR4_ECOLI), *C. ammoniagenes* (B.-M. Sjöberg, personal communication), *M. tuberculosis* (RIR2_MYCTU), *M. pneumonia* (RIR2_MYCPN), *M. genitalium* (RIR2_MYCGE), *E. coli* Ia (RIR2_ECOLI), and mouse (RIR2_MOUSE). The alignment was formatted using ALscript (*63*).

most exposed of the totally conserved R2 residues and has been proposed to interact with R1 (*49*). It is certainly located in an important position and may participate in electron transfer. No mutagenesis studies have so far been performed on this arginine in any R2 protein. An interesting feature is the connection between the two histidines which ligand the irons (Figure 9). Two water molecules connect His195 with Asp191 in the radical transfer pathway; in *E. coli*, the same connection is made by a Gln. This link might be important during reconstitution of the tyrosyl radical and the radical transfer during substrate reduction.

The C-terminal part of the protein is not visible in any of the R2 proteins, and from NMR studies is shown to be highly mobile (*50*, *51*). This flexible part of the protein has been demonstrated to be involved in the radical transfer between the tyrosyl radical and the active site in R1 (*59*), particularly, a tyrosine that is conserved in all R2 proteins. This tyrosine is preceded by a glutamic acid that has also been suggested to be involved in the radical transfer, but the role of this residue is less well-established; however, the E350A mutant is 240 times less efficient (*59*). In R2F, this Glu is replaced by a Ser, and in this part of the sequence the only carboxylate is located three residues earlier.

Structural Implications for the nrdF Family of R2 Proteins. Six different *nrdF* sequences are present in the databases that have strong similarities to each other. The sequence identity between the R2F sequences from *S. typhimurium* and other R2F sequences is 88% to the *E. coli*, 42% to the *B. subtilis*, 65% to the *M. tuberculosis*, 49% to the *M. genitalium*, and 50% to the *M. pneumonia* R2F sequences. The aligned sequences are shown in Figure 10. Of these sequences, the *B. subtilis*, the *E. coli* class Ib, and the *M. tuberculosis* sequences contain all the residues which have been related to activity. Surprisingly, both the *M. genitalium* and the *M. pneumonia* sequences lack three of the iron ligands; instead of Glu98 these sequences have Val, instead of Glu157 these sequences have Pro, and instead of Glu192 they have Lys. These sequence differences are incompatible with the formation of an iron site. At the corresponding position as the last one (corresponding to Glu238 in *E. coli* R2), there is an Arg in the unusual yeast R2 form called RNR4 (*60*, *61*). This R2 is inactive by itself but necessary for the formation of an active enzyme of RNR1 and RNR2 (*61*).

The recently determined sequence of the manganese-containing ribonucleotide reductase from *C. ammoniagenes* (*34*) is 66% identical with the *E. coli* class Ib and *S. typhimurium* R2F. It contains all functional residues including all the metal ligands. The second sphere ligands of the metal center and the environment of the tyrosyl radical are also the same so the differences between the two structures should be very subtle; a sphere around the iron center of 9 Å has identical residues. This poses the question of how metal specificity is selected within the family. In view of the similarities between the R2F structure in the reduced state and the Mn-substituted *E. coli* R2, the metal site in the R2F structure seems ideally suited for Mn binding.

ACKNOWLEDGMENT

We thank Irmgard Kurland for assistance with the expression of the R2F protein.

REFERENCES

1. Thelander, L., and Reichard, P. (1979) *Annu. Rev. Biochem. 48*, 133−158.
2. Hendricks, S. P., and Mathews, C. K. (1997) *J. Biol. Chem. 272*, 2861−2865.
3. Lin, A., and Elford, H. (1980) *J. Biol. Chem. 255*, 8523−8528.
4. Markert, M. (1991) *Immunodefic. Rev. 3*, 45−81.
5. Yoshioka, A., Tanaka, S., Hiraoka, O., Koyama, Y., Hirota, Y., and Wataya, Y. (1987) *Biochem. Biophys. Res. Commun. 146*, 258−264.
6. Kunz, B. A. (1988) *Mutat. Res. 200*, 133−147.
7. Meuth, M. (1984) *Mutat. Res. 126*, 107−112.
8. Meuth, M. (1989) *Exp. Cell. Res. 181*, 305−316.
9. Caras, I. W., and Martin, D. W. J. (1988) *Mol. Cell. Biol. 8*, 2698−2704.
10. Reichard, P. (1993) *Science 260*, 1773−1777.
11. Sjöberg, B.-M. (1997) *Structure Bonding 88*, 139−173.
12. Gräslund, A., Sahlin, M., and Sjöberg, B.-M. (1985) *Environ. Health Perspect. 64*, 139−149.
13. Licht, S., Gerfen, G. J., and Stubbe, J. (1996) *Science 271*, 477−481.
14. Sun, X. Y., Ollagnier, S., Schmidt, P. P., Atta, M., Mulliez, E., Lepape, L., Eliasson, R., Gräslund, A., Fontecave, M., Reichard, P., and Sjöberg, B. M. (1996) *J. Biol. Chem. 271*, 6827−6831.
15. Ollagnier, S., Mulliez, E., Gaillard, J., Eliasson, R., Fontecave, M., and Reichard, P. (1996) *J. Biol. Chem. 271*, 9410−9416.
16. Lin, A.-N. I., Ashley, G. W., and Stubbe, J. (1987) *Biochemistry 26*, 6905−6909.
17. Åberg, A., Hahne, S., Karlsson, M., Larsson, Å., Ormö, M., Åhgren, A., and Sjöberg, B.-M. (1989) *J. Biol. Chem. 264*, 12249−12252.
18. Mao, S. S., Holler, T. P., Yu, G. X., Bollinger, J.-M., Booker, S., Johnston, M. I., and Stubbe, J. (1992) *Biochemistry 31*, 9733−9743.
19. Holmgren, A. (1989) *J. Biol. Chem. 264*, 13963−13966.
20. Fontecave, M., Eliasson, R., and Reichard, P. (1989) *J. Biol. Chem. 264*, 9164−9170.
21. Jordan, A., Gibert, I., and Barbé, J. (1994) *J. Bacteriol. 176*, 3420−3427.
22. Jordan, A., Pontis, E., Atta, M., Krook, M., Gibert, I., Barbé, J., and Reichard, P. (1994) *Proc. Natl. Acad. Sci. U.S.A. 91*, 12892−12896.
23. Jordan, A., Aragall, E., Gibert, I., and Barbé, J. (1996) *Mol. Microbiol. 19*, 777−790.
24. Eliasson, R., Pontis, E., Jordan, A., and Reichard, P. (1996) *J. Biol. Chem. 271*, 26582−26587.
25. Allard, P., Barra, A. L., Andersson, K. K., Schmidt, P. P., Atta, M., and Gräslund, A. (1996) *J. Am. Chem. Soc. 118*, 895−896.
26. Jordan, A., Åslund, F., Pontis, E., Reichard, P., and Holmgren, A. (1997) *J. Biol. Chem. 272*, 18044−18050.
27. Jordan, A., Gibert, I., and Barbé, J. (1995) *Gene 167*, 75−79.
28. Yang, F. D., Lu, G. Z., and Rubin, H. (1994) *J. Bacteriol. 176*, 6738−6743.
29. Jordan, A., Pontis, E., Åslund, F., Hellman, U., Gibert, I., and Reichard, P. (1996) *J. Biol. Chem. 271*, 8779−8785.
30. Scotti, C., Valbuzzi, A., Perego, M., Galizzi, A., and Albertini, A. M. (1996) *Microbiology 142*, 2995−3004.
31. Fraser, C. M., Gocayne, J. D., White, O., Adams, M. D., Clayton, R. A., Fleischmann, R. D., Bult, C. J., Kerlavagne, A. R., Sutton, G., Kelley, J. M., Fritchman, J. L., Weidman, J. F., Small, K. V., Sandusky, M., Fuhrmann, J., Nguyen, D., Utterback, T. R., Saudek, D. M., and Venter, J. C. (1995) *Science 270*, 397−403.
32. Himmelreich, R., Plagens, H., Hilbert, H., Reiner, B., and Herrmann, R. (1997) *Nucleic Acids Res. 25*, 701−712.
33. Willing, A., Follmann, H., and Auling, G. (1988) *Eur. J. Biochem. 170*, 603−611.
34. Fieschi, F., Torrents, E., Toulokhonova, L., Jordan, A., Hellman, U., Barbé, J., Gibert, I., Karlsson, M., and Sjöberg, B. (1998) *J. Biol. Chem. 273*, 4329−4337.

35. Sambrook, J., Fritsch, E. F., and Maniatis, T. (1989) *Molecular cloning: A laboratory manual*, 2nd ed., Cold Spring Harbor Laboratory, Cold Spring Harbor, NY.
36. Otwinowski, Z. (1993) *Proceedings of the CCP4 study weekend*, pp 56−62, Daresburry Laboratories, Warrington, U.K.
37. Knight, S. (1989) Thesis, Swedish University of Agricultural Sciences.
38. de La Fortelle, E., and Bricogne, G. (1997) *Methods Enzymol. 276*, 442−494.
39. Abrahams, J. P., and Leslie, A. G. W. (1996) *Acta Crystallogr. D52*, 30−42.
40. Cowtan, K. (1994) *Joint CCP4 ESF-EACBM Newsletter Protein Crystallogr. 31*, 34−38.
41. Jones, T. A., Zou, J. Y., Cowan, S. W., and Kjeldgaard, M. (1991) *Acta Crystallogr. 47*, 110−119.
42. Adams, P. D., Pannu, N. S., Read, R. J., and Brünger, A. T. (1997) *Proc. Natl. Acad. Sci. U.S.A. 94*, 5018−5023.
43. Brünger, T. A., Kuriyan, J., and Karplus, M. (1987) *Science 235*, 458−460.
44. Brünger, A. T., Krukowski, A., and Erickson, J. (1990) *Acta Crystallogr. A46*, 585−593.
45. Brünger, A. T. (1992) *Nature 355*, 472−474.
46. Brünger, A. T. (1997) *Methods Enzymol. 276*, 558−580.
47. Pannu, N. S., and Read, R. J. (1996) *Acta Crystallogr. A52*, 659−668.
48. Nordlund, P., Sjöberg, B.-M., and Eklund, H. (1990) *Nature 345*, 593−598.
49. Nordlund, P., and Eklund, H. (1993) *J. Mol. Biol. 232*, 123−164.
50. Lycksell, P. O., Ingemarson, R., Davis, R., Gräslund, A., and Thelander, L. (1994) *Biochemistry 33*, 2838−2842.
51. Lycksell, P. O., and Sahlin, M. (1995) *FEBS Lett. 368*, 441−444.
52. Kauppi, B., Nielsen, B. A., Ramaswamy, S., Larsen, I. K., Thelander, M., Thelander, L., and Eklund, H. (1996) *J. Mol. Biol. 262*, 706−720.
53. Atta, M., Nordlund, P., Åberg, A., Eklund, H., and Fontecave, M. (1992) *J. Biol. Chem. 267*, 20682−20688.
54. Logan, D. T., Su, X. D., Åberg, A., Regnström, K., Hajdu, J., Eklund, H., and Nordlund, P. (1996) *Structure 4*, 1053−1064.
55. Davydov, R., Kuprin, S., Gräslund, A., and Ehrenberg, A. (1994) *J. Am. Chem. Soc. 116*, 11120−11128.
56. Hendrich, M. P., Elgren, T. E., and Que, L. J. (1991) *Biochem. Biophys. Res. Commun. 176*, 705−710.
57. Lindqvist, Y., Huang, W. J., Schneider, G., and Shanklin, J. (1996) *EMBO J. 15*, 4081−4092.
58. Himo, F., Gräslund, A., and Eriksson, L. (1997) *Biophys. J. 72*, 1556−1567.
59. Climent, I., Sjöberg, B.-M., and Huang, C. Y. (1992) *Biochemistry 31*, 4801−4807.
60. Huang, M. X., and Elledge, S. J. (1997) *Mol. Cell. Biol. 17*, 6105−6113.
61. Wang, P. J., Chabes, A., Casagrande, R., Tian, X. C., Thelander, L., and Huffaker, T. C. (1997) *Mol. Cell. Biol. 17*, 6114−6121.
62. Kraulis, P. (1991) *J. Appl. Crystallogr. 24*, 946−950.
63. Barton, G. J. (1993) *Protein Eng. 6*, 37−40.

BI981380S